Polymer 51 (2010) 5135–5144

Contents lists available at ScienceDirect

Polymer

journal homepage: www.elsevier.com/locate/polymer

Effects of genistein modification on miscibility and hydrogen bonding interactions in poly(amide)/poly(vinyl pyrrolidone) blends and membrane morphology development during coagulation

Chandrasekaran Neelakandan, Thein Kyu*

Department of Polymer Engineering, University of Akron, Akron, OH 44325, USA

ARTICLE INFO

Article history:
Received 28 June 2010
Received in revised form
8 September 2010
Accepted 12 September 2010
Available online 18 September 2010

Keywords:
Miscibility
Phytochemicals
Coagulation driven phase separation

ABSTRACT

Miscibility characteristics of poly(amide):poly(vinyl pyrrolidone) (PA:PVP) blends containing a soybean-derived phytochemical called "genistein" have been investigated using differential scanning calorimetry (DSC) and polarized optical microscopy (POM). The occurrence of hydrogen bonding in the binary PA/genistein (PA/G) and PVP/genistein (PVP/G) pairs as well as their ternary blends has been confirmed by Fourier transformed infrared spectroscopy (FTIR). On the basis of DSC and POM data, the morphology phase diagram of PA:PVP/G blends is mapped out, which consisted of various coexistence regions such as isotropic, liquid + liquid, liquid + crystal, liquid + liquid + crystal, and solid crystal regions. Subsequently, PA:PVP membranes modified with genistein were prepared by coagulation via solvent (dimethyl sulfoxide, DMSO) and non-solvent (water) exchange. Addition of genistein reduced the miscibility gap of the PA/DMSO/water system. The actual amounts of genistein in the final membranes have been quantified as a function of the genistein in feed. Of particular interest is the development of the gradient cross-sectional porous channels, showing the progressively larger diameters from the surface to the bottom substrate with the progression of solvent/non-solvent exchange or solvent power. Scanning electron microscopy (SEM) investigation of the morphologies of the modified membranes revealed that genistein crystals were embedded on the membrane surface as well as in the cross-section even at a very low feed concentration of genistein. A schematic of a coagulation pathway was inscribed inside a prism phase diagram in order to comprehensively illustrate the formation of genistein modified PA:PVP membranes through the solvent/non-solvent exchange process followed by drying.

1. Introduction

The scope of membrane technology has expanded beyond the traditional separation processes such as reverse osmosis, ultrafiltration, microfiltration, and gas separation [1], which currently encompasses drug delivery, biodegradable membranes for tissue engineering, and among others. The biomedical focus on membrane technology has revived the academic and industrial research interests of this relatively mature field. One of earliest biomedical applications of membranes pertains to artificial kidneys or hemodialysis. Hemodialysis (HD) technology sustains the life of millions of patients worldwide whose kidney functions are partially or fully impaired [2]. In HD, impure blood from the patient is pumped through polymeric hollow fiber membranes for repeated cycles in order to reduce the concentration of uremic toxins in blood. Typical contact time of hemodialysis patients' blood with synthetic polymer surface is approximately 3–4 h for each session and 3–4 sessions per week [3]. Although, HD is a life-sustaining treatment, two of its important long-term complications, viz., dialysis induced oxidative stress (DIOS), and membrane induced inflammation (MII) reveal the double-edged nature of HD. In the long run, DIOS and MII act in tandem and cause cardiovascular disorder that contributes to 40% mortality in hemodialysis patients. DIOS is initiated when the excess production of oxygen radicals overcomes the natural anti-oxidant defense mechanisms of the body [4], whereas MII causes undesirable immune response [5]. The bio-incompatibility of the synthetic polymer surface has been singled out as a significant source and has been implicated towards the aforementioned pitfalls of HD treatment. Therefore, there exists an imminent demand for functional HD membranes, which could potentially suppress these long-term ill-effects of HD.

Recently, we have engaged in investigations of a group of plant-derived chemicals called phytochemicals, which have been shown to possess invaluable health benefits [6–8]. The natural origin, abundant availability, lower toxicity, and ease of extraction have been the

* Corresponding author. Tel.: +1 330 972 6672; fax: +1 330 258 2339.
E-mail address: tkyu@uakron.edu (T. Kyu).

0032-3861/$ – see front matter © 2010 Elsevier Ltd. All rights reserved.
doi:10.1016/j.polymer.2010.09.030

attractive features of phytochemicals, which provoked our interests towards their utilization for development of novel materials. Genistein, a soybean-derived phytochemical was chosen for use in functional HD membranes because of its well-known anti-oxidant [9,10] and anti-inflammatory [11,12] properties. Poly(amide):poly(vinyl pyrrolidone) (PA:PVP) pair was selected as the polymer matrix because of its proven tracked record in the current HD membrane technology [13].

In this article, we first establish the miscibility characteristics of PA:PVP/genistein ternary blends based on differential scanning calorimetry and cloud point measurements. We then investigate the effect of genistein incorporation on the surface and cross-sectional membrane morphologies driven by solvent/non-solvent exchange. Of particular interest is the development of the cascading gradient porous morphology in the cross-section embedded with genistein crystals. A coagulation pathway in relation to a prism phase diagram is presented in order to provide guidance to the morphology evolution of the final PA:PVP/genistein membranes.

2. Experimental section

2.1. Materials

TROGAMID® T5000 (Mn = 20,000 and Mw = 63,000) [14,15], an aromatic poly(amide) was kindly provided by Degussa Corporation (NJ, USA). PVP (Mw = 40,000) was purchased from Sigma–Aldrich, (MO, USA). A reagent grade DMSO, purchased from Sigma–Aldrich (MO, USA), was used as a common solvent without further purification. Genistein (>98% purity) was purchased from MDidea Exporting Division (YinChuan, China). Reverse osmosis grade water was utilized as non-solvent for membrane formation.

2.2. Methods

Thermal stability of pure genistein was determined using a thermogravimetric analyzer (TGA) (TA Instruments, Model 2050). In the TGA experiments, the samples were heated at a rate of 10 °C/min from 100 °C to 600 °C in a nitrogen atmosphere. The temperature at which the 5% weight loss occurred was regarded as the degradation temperature. The glass transition temperatures (T_g) for pure components and blends were measured at a heating rate of 10 °C/min using TA Instruments (Model 2920) differential scanning calorimeter (DSC) calibrated for temperature and enthalpy using indium standard having a melting point of 165.5 °C. For DSC experiments, homogeneous solutions of PA, PVP, genistein and their blends were prepared in DMSO (common solvent) followed by solvent removal under vacuum at 150 °C for 24 h. The samples were enclosed tightly in hermitic aluminum DSC pans and heated up to 250 °C to remove thermal history and rerun for a second time up to 320 °C. The second run data was used to identify the glass transition temperature and crystal melting temperature.

For Fourier transformed infrared spectroscopy (FTIR) investigations, samples were solution cast on KBr discs and then dried under vacuum at 150 °C for 24 h. Infrared spectra were acquired on an FTIR spectrometer (Thermo Scientific Nicolet 380) at a resolution of 4 cm^{-1} averaged over 32 scans. FTIR data were collected at 100 °C in order to minimize the effects of moisture. Regarding POM experiments, thin films (~10 μm) were cast on glass substrates followed by a solvent removal procedure described above. POM images were recorded using an optical microscope (BX60, Olympus) equipped with a 35 mm digital camera (EOS 400D, Canon).

Ternary phase diagram for PA/DMSO/water system was constructed by determining the cloud points via titration of PA solutions with water. PA solutions of varying concentrations were prepared by mixing PA with DMSO and homogenizing for 24 h.

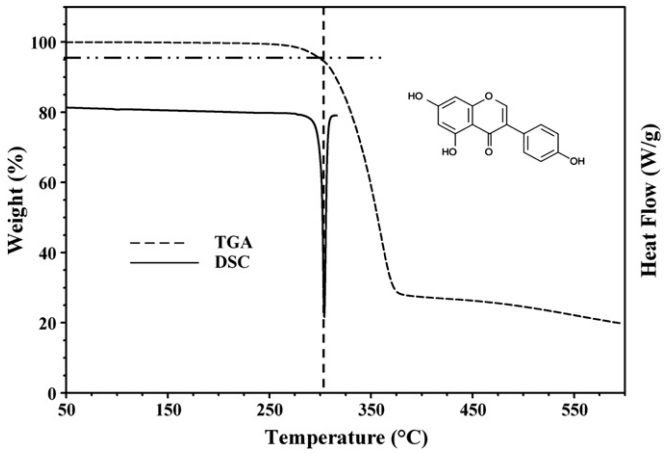

Fig. 1. Overlay of DSC and TGA thermograms for genistein illustrating the thermal decomposition of genistein occurring at its melting point. The inset shows the chemical structure of genistein.

Subsequently, a known quantity of water was gradually added to each solution while maintaining the solutions at 25 °C. The amount of water that was required to turn the homogeneous solutions turbid was regarded as the cloud point. In order to establish the phase diagram for genistein/DMSO/water system, DMSO and water were mixed at various compositions in a thermostatted bath maintained at 25 °C. Small quantities of genistein were incrementally added to this mixture while allowing sufficient time between each addition to ensure equilibrium. Genistein was added until a saturation point was reached and the concentration at which genistein can no longer be dissolved in the solution was considered as the phase transition point, which separated the isotropic phase from the isotropic + crystal coexistence phases. In order to determine the effect of genistein addition on PA/DMSO/water phase diagram, cloud point experiments were carried out as described above with the exception that each solution was mixed with genistein such that PA/genistein (PA/G) ratio in each solution remained constant (for e.g., 90/10, 80/20 and 70/30 PA/G).

In order to cast membranes, PA pellets were vacuum-dried at 80 °C for 24 h and subsequently dissolved in DMSO. The solutions used to cast membranes hereafter are termed as 'feed solution'. In the preparation of genistein modified membranes, appropriate amounts of genistein were added to the feed solution. The solutions were homogenized for 48 h and the entrapped air was removed under vacuum at room temperature. The homogeneous solutions were then cast in the form of a film of pre-determined thickness on a pre-cleaned glass plate followed by immersion into reverse osmosis grade water (i.e., non-solvent) maintained at 25 °C. The coagulated membranes, which peeled-off from the glass plate, were rinsed with excess water and vacuum-dried at room temperature. For the SEM study, dried membranes samples were fractured in liquid nitrogen and then sputtered with silver using a sputter coater (Emitech, Model K575X) and analyzed with field emission scanning electron microscope (JEOL-Model JSM-7401F). The sample surfaces were cleaned gently with compressed air before sputtering. SEM micrographs were taken at three different areas that were representative of the whole sample.

3. Results and discussion

3.1. Miscibility characteristics of PVP/G and PA/G binary blends

In our recent work [16], we reported that the PA:PVP blends were completely miscible in the entire composition range. It was also

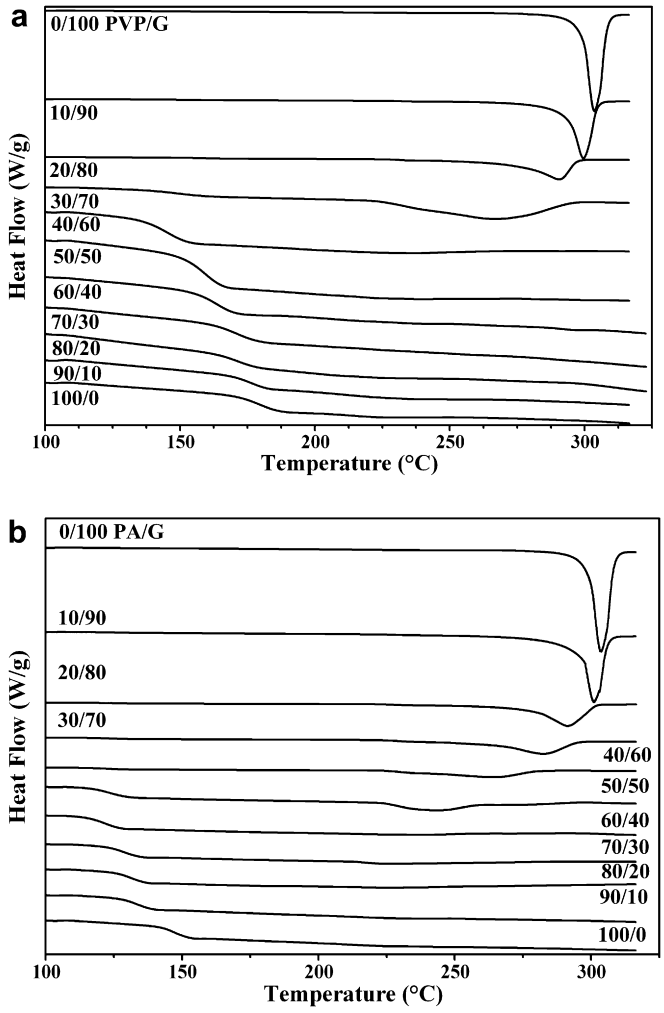

Fig. 2. Second run DSC thermograms for (a) PVP/genistein and (b) PA/genistein blends showing single Tg and its systematic movement to lower temperatures with increasing amount of its polymer counterparts and the associated depression of crystal melting peak of the genistein crystals.

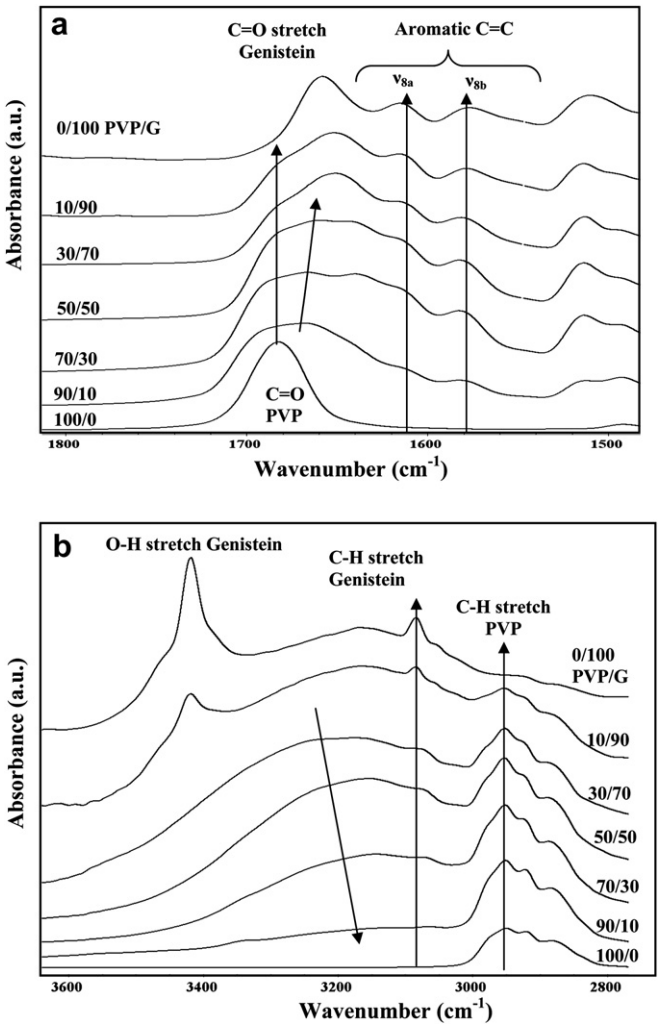

Fig. 3. FTIR spectra recorded at 100 °C for PVP/genistein blend (a) in the range 1500–1800 cm^{-1} demonstrates hydrogen bonding formation as shown by the systematic movement of carbonyl band of the blends to lower wavenumbers and (b) in the 2700–3600 cm^{-1} range for PVP/mangiferin blends showing the shift of broad O–H band of genistein bands to lower wavenumbers. The aromatic C=C band of genistein shows no spectral shift.

demonstrated that the occurrence of hydrogen bonding interactions between the two polymers contributed towards such enhanced miscibility between PA and PVP. Fig. 1 shows the overlaid plots of DSC and TGA thermograms of pure genistein along with its chemical structure (inset). As typical for the small molecule crystals, the melting peak of genistein is sharp. This DSC peak at 306 °C coincided with the onset of thermal degradation of genistein in the TGA thermogram, which accidentally corresponds to the 5% weight loss that has been used as a standard for polymer degradation temperature.

The solvent cast PVP/G samples were transparent to naked eyes, but possessed a golden tinge owing to the inherent color of genistein. As shown in Fig. 2(a), a single glass transition is evident in each DSC scan of the PVP/G blends, showing systematical movement of the T_g to lower temperatures with increasing genistein loading. This trend implies that T_g of genistein, if any, might be located at a lower temperature as compared to that of the PVP. The reduction in the T_g of the blends also suggests that genistein is possibly acting as a diluent to the PVP matrix. Another noteworthy feature in Fig. 2(a) is the depressed trend of the melting peak (T_m) of genistein crystals in the PVP/G blends with PVP addition, but it eventually disappeared as PVP concentration increased further (i.e., >30 wt % PVP). The observed systematic movement of T_g and lowering of T_m with PVP/G blend ratio are the typical signatures of blend miscibility of the pair in the amorphous state.

The PA/G blend shows considerable similarity to that of PVP/G pair. Visually, all PA/G blends were also transparent to naked eyes with a golden tinge color of genistein. The DSC thermograms of PA/G samples exhibited a single T_g, which consistently shifted to lower temperatures with increasing genistein concentration up to 40 wt % genistein (Fig. 2(b)). The depression of the melting transitions can also be discerned in the PA/G blends, but the genistein crystal melting peak persisted to a higher PA loading relative to that of the PVP/G blends.

In order to probe the occurrence of any specific interactions between PVP and genistein, FTIR spectra were collected at 100 °C. It should be pointed out that PVP is not a self-associating polymer, but contains functional groups (C=O) that can form hydrogen bonds with hydroxyl groups of genistein through electron donor–acceptor type of interaction. Fig. 3(a) and (b) illustrates the FTIR spectra of PVP/G blends in the 1500–1800 and 2800–3600 cm^{-1} range, respectively. The FTIR analysis of the PVP/genistein system is relatively straightforward because only genistein can self-associate. Pure genistein shows a sharp band at 3425 cm^{-1} corresponding to the

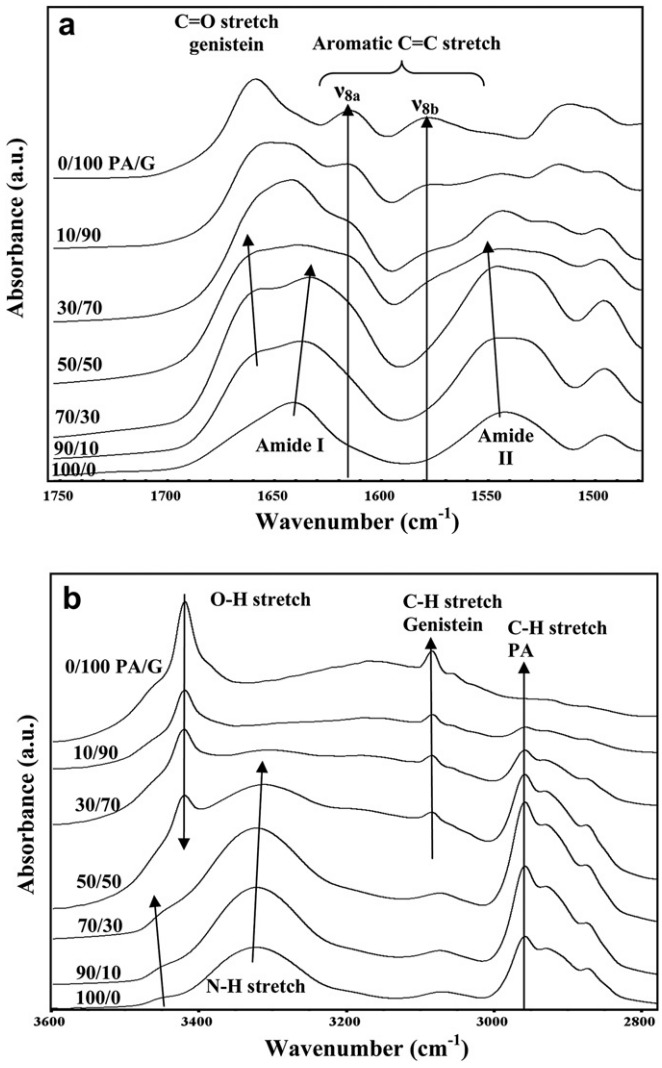

Fig. 4. FTIR spectra recorded at 100 °C for PA/genistein blends (a) in the range of 1500–1800 cm^{-1} demonstrates hydrogen bonding formation as shown by the systematic movement of amide I band of PA to lower wavenumbers and amide II band to higher wavenumbers (b) in the 2700–3600 cm^{-1} range for PA/mangiferin blends illustrating the shift of N–H stretching to lower wavenumbers.

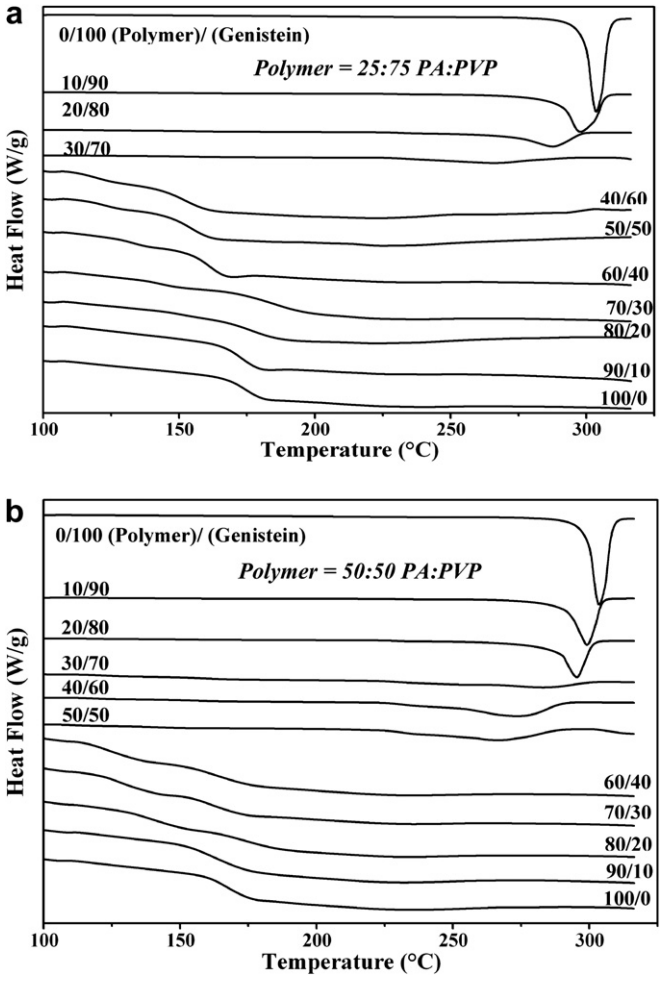

Fig. 5. Second run DSC thermograms for PA:PVP/genistein ternary blends with (a) 25:75 PA:PVP ratio and (b) 50:50 PA:PVP ratio exhibiting a single T_g shifting systematically to lower temperature at low genistein loading and two T_gs at medium genistein loading indicating showing liquid–liquid phase separation. Liquid–solid phase segregation can be seen at high genistein concentrations.

O–H stretching, whereas PVP has no such band in the corresponding region (Fig. 3(b)). As the concentration of PVP is increased the sharp hydroxyl band becomes broader and shifts to lower wavenumbers while reducing its magnitude as evident from Fig. 3(b). This shift of O–H stretching band for PVP/G blends is seemingly governed by the competition between hydroxyl–hydroxyl (self) of genistein and hydroxyl–carbonyl (interspecies or cross) interactions between PVP and genistein. While the addition of PVP is expected to free up some of the self-associated hydroxyl groups of genistein, the freed O–H groups readily forms hydrogen bonds with C=O of PVP. The corresponding effect can be explicitly seen in the carbonyl spectral region (Fig. 3(a)). Upon addition of genistein to PVP (i.e., 90/10 PVP/G), the C=O band splits into free C=O band and hydrogen bonded C=O band. The free C=O band of PVP (1682 cm^{-1}) remains stationary which is consistent with the fact that PVP is not self-associating. The second band appears to move to a lower wavenumber with increasing PVP composition and the position of the band is in between the C=O of PVP (1682 cm^{-1}) and C=O of genistein (1658 cm^{-1}). This observation suggests that only a fraction of the C=O groups of PVP forms hydrogen bonds with O–H groups of genistein. The 1682 cm^{-1} band can be clearly seen in all the PVP/G blends. However, the shift of the hydrogen bonded C=O band can no longer be observed beyond 50/50 PVP/G possibly due to the formation of crystals at higher genistein concentrations. These trends are consistent with literature studies involving interactions between PVP and hydroxyl groups [17,18]. The characteristics bands that are not involved in any specific interactions such as aromatic C=C stretching bands (Fig. 3(a)) and C–H stretching vibrations of genistein and PVP (Fig. 3(b)) show no movement as expected.

Fig. 4(a) and (b) illustrates the FTIR spectrum of PA/G blends in the 1500–1800 and 2800–3600 cm^{-1} range, respectively. In this case, both PA and genistein are self-associating components, capable of forming intra-and inter-molecular hydrogen bonding. The 1640 cm^{-1} band of PA corresponds mostly to the self-associated amide I groups (i.e., hydrogen bonding within the same species) [19–21]. As seen in Fig. 4(a), the addition of genistein causes amide I band of PA to shift to lower wavenumbers due hydrogen bonding with the hydroxyl groups of genistein. On the other hand, a second band appears around 1660 cm^{-1}, which corresponds to C=O of genistein or to C=O groups of PA that are being freed up due to blending with genistein. In either case, this band appears to shift to a higher wavenumber indicating the release of self-associated groups. In contrast, the aromatic C=C band does not show any movement since it is not involved in any specific interaction. The

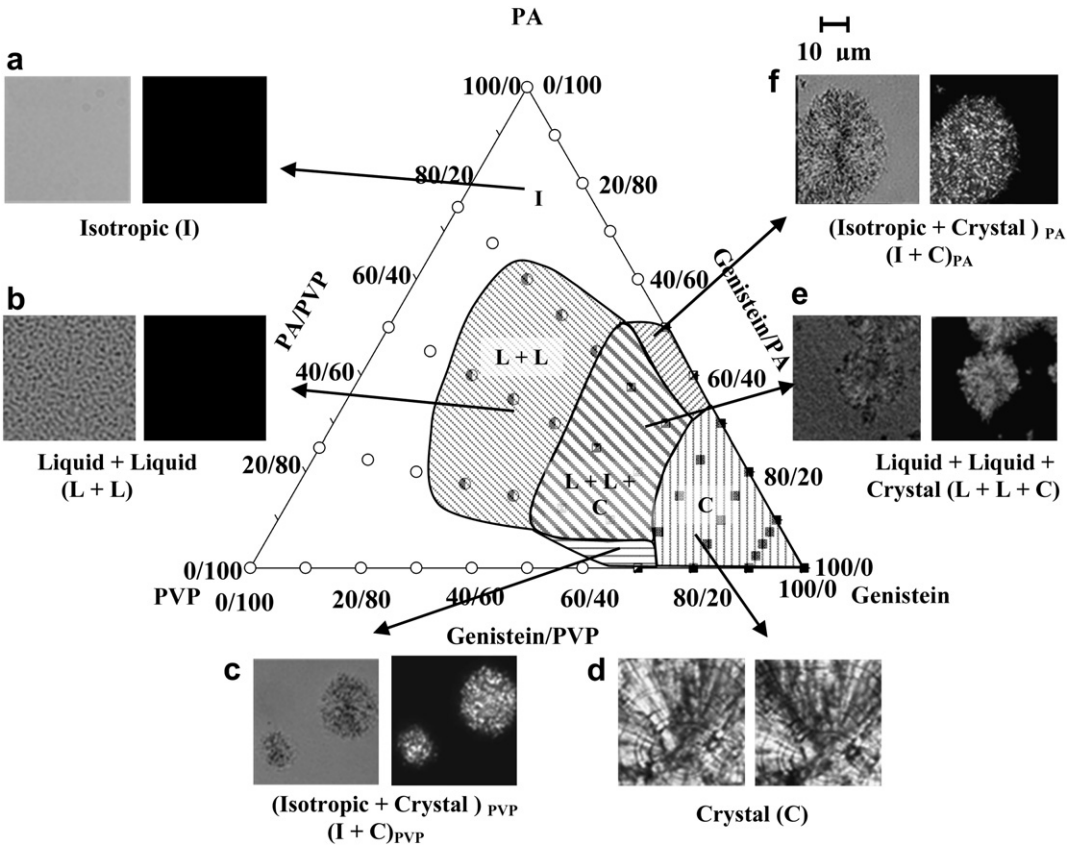

Fig. 6. Ternary morphology phase diagram of PA:PVP/genistein blends, showing various coexistence regions (labeled by different shading). Polarized and unpolarized of optical microscope images representing typical morphologies of each region are shown in relation to the ternary phase diagram. Keys for labels are: I = isotropic (unfilled circles), C = crystal (filled squares), (I + C)PVP = coexistence of isotropic and crystals for PVP-rich compositions (left half-filled squares), (I + C)PA = coexistence of isotropic and crystal for PA-rich compositions (right half-filled squares), L + L = liquid + liquid (half-filled circles), L + L + C = liquid + liquid + crystal (hour glass-filled circles). The phase boundary lines were drawn by hand to guide the eyes.

amide II band shifts to higher wavenumbers, which is also consistent with interactions of amide and hydroxyl groups [22]. It has been generally accepted that the formation of a stronger hydrogen bond tends to increase the wavenumber of a donor deformation vibration like $-NH_2$ scissoring (i.e., amide II) while it decreases the wavenumber of an acceptor vibration such as the C=O stretching [23]. This is because the amide II band which corresponds to the scissoring mode of vibration is stiffened by the formation of hydrogen bonds. On the other hand, formation of hydrogen bonds with the C=O bond tends to draw electrons via attractive interactions resulting in the reduction in wavenumber of the C=O stretching. It is more difficult to analyze the FTIR band shifts in the N–H stretching region (Fig. 4(b)) due to the overlap of O–H and N–H bands. However, it can be clearly seen that the N–H stretching band at 3322 cm^{-1} shifts to a lower wavenumber due to interactions with O–H or C=O of genistein while free N–H band 3444 cm^{-1} shifts to higher wavenumber indicating the release of N–H groups that were self-associated. The sharp O–H band marginally also shifts to a lower wavenumber further confirming our hypothesis that cross-hydrogen bonding occurs between PA and genistein. The possible interactions, in these blends include N–H···C=O (self), N–H···C=O (cross), N–H···O–H (cross) and O–H···O–H (self) interactions.

3.2. Miscibility characteristics of PA:PVP/genistein ternary blends

Fig. 5(a) and (b) exhibits the DSC thermograms of PA:PVP/genistein blends in which the PA:PVP ratio has been fixed at 25:75 and 50:50 respectively. Upon addition of genistein 25:75 PA:PVP blends, a single glass transition is discernible only up to 30 wt% of genistein, beyond which the system undergoes liquid–liquid phase separation as manifested by the appearance of two glass transition temperatures corresponding to PA-rich and PVP-rich phases. The dual glass temperatures were detected up to 60 wt % genistein, but it becomes less distinct with further increase of genistein, which may be suppressed by the appearance of crystal melting transition (Fig. 5(a)). For the case of 50:50 PA:PVP blends, liquid–liquid phase separation begins to take place even at 20 wt % genistein as shown in Fig. 5(b). This phase separated trend continues with further increase of genistein concentration in which the dual glass transitions shifted to lower temperatures. At very high genistein loadings, crystal melting peaks were observed along with dual T_gs suggesting liquid + liquid + crystal coexistence phase. A competing trend of liquid–liquid phase separation with liquid–solid phase transition was also observed for the PA-rich blend such as 75:25 PA:PVP (data not shown).

The phenomena of liquid–liquid phase separation and solid–liquid phase transition were also independently confirmed by POM studies. As mentioned before, PA/G and PVP/G blends were transparent to naked eyes showing no indication of liquid–liquid phase separation at low genistein compositions. Further increase in genistein concentration resulted in crystallization of genistein showing the large spherulitic structures in the continuum of isotropic liquid signifying the isotropic + crystal (liquid + solid) coexistence phase. At very high concentrations of genistein, the entire field of optical microscope view was filled with solid crystals. In the case of PA:PVP blends, the addition of genistein revealed liquid–liquid phase separated domains in addition to isotropic single phase and crystal + liquid coexistence phases.

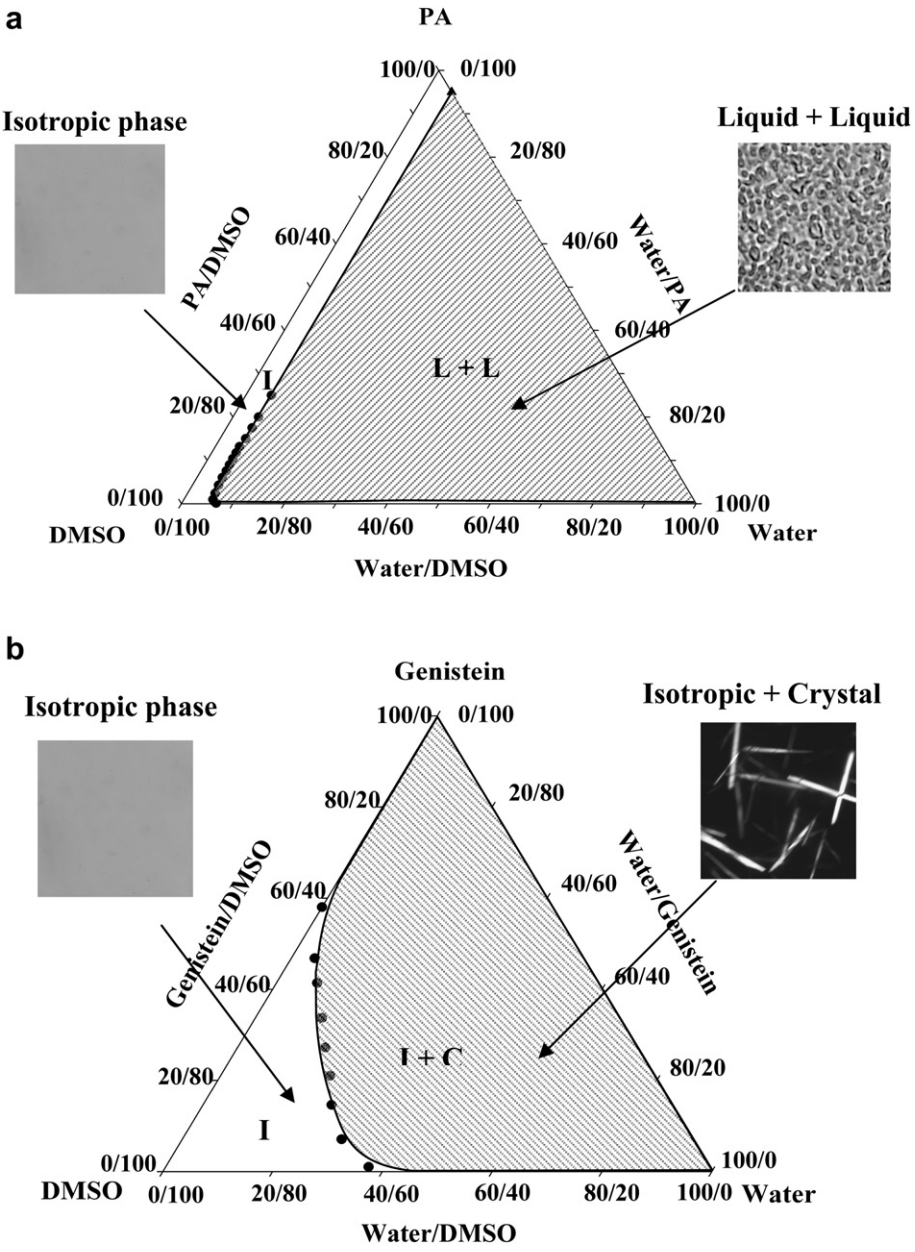

Fig. 7. (a) Ternary phase diagram for PA/DMSO/Water obtained by cloud point measurements (●) exhibiting liquid–liquid immiscibility gap. The ▲ on water/PA axis represents the data reported in literature based on water absorption studies. Optical micrographs obtained under the parallel polarizers showing the isotropic liquid without any texture (left) and phase separated structure (right). (b) Ternary phase diagram for genistein/DMSO/water system demonstrating the isotropic + crystal coexistence region along with the corresponding optical micrographs showing the needle-like crystals of genistein dispersed in an isotropic matrix (right) and the textureless morphology signifying the isotropic phase (left).

In order to comprehensively map the miscibility characteristics of PA:PVP/genistein blends, a ternary morphology phase diagram was established based on information gathered from DSC along with the optical micrographs of the POM experiments (Fig. 6). The symbols represent the data points obtained from the DSC. Different types of shading were employed to delineate various coexistence regions, showing single phase (I) (open circles), solid crystal phase (C) (filled squares), liquid + solid phase (I + C) (half-filled squares), two liquid coexistence phases (L + L) (half-filled circles) and the liquid + liquid + crystal solid phases (L + L + C) (hour glass-filled square). *The phase boundary lines were drawn by hand to guide the eyes.* Typical bicontinuous morphology of a liquid–liquid phase separated region is evident as displayed in the optical micrograph (b) to the left hand side of the phase diagram. This co-continuous structure is a typical signature of spinodal decomposition, although it is by no means a proof. In the region marked 'L + L + C' region (micrograph (e)), the crystal aggregates in the form of spherulites were found to be dispersed in a continuum of liquid–liquid phase separated matrix, which is in good agreement with the preceding DSC results. Finally, in the crystal region, the whole field of view of POM was filled with solid crystals of genistein (micrograph (d)).

3.3. Phase diagrams for membrane formation and development of membrane morphology

Fig. 7(a) shows the ternary phase diagram for PA/DMSO/water system constructed based on the cloud point measurement, exhibiting a narrow isotropic gap (unshaded region) and a liquid + liquid

coexistence region (shaded region). The textureless optical micrograph on the left is characteristic of an isotropic region, but the picture on the right shows liquid–liquid phase separated morphology. Owing to the very high viscosity of polymer solutions (i.e., >30 wt% PA), homogenization of the mixture after water addition became impractical. Hence, the immiscibility gap was extrapolated to the water/PA axis (5 wt %) in accordance with the reported water absorption measurements [24]. Before embarking on fabrication of phytochemicals modified polymer membranes, it is utmost important to understand the miscibility characteristics of pure genistein in a mixture of DMSO and water. A ternary phase diagram of genistein/DMSO/water mixture was constructed as described in the experimental methods section. As depicted in Fig. 7(b), the ternary phase diagram for genistein/DMSO/water consisted of an isotropic single phase at higher DMSO concentrations and a crystal + isotropic coexistence gap at lower DMSO contents. This isotropic + crystal coexistence region (i.e., crystallization) was confirmed by the optical microscope image shown on the right hand side of the phase diagram, showing the needle-like crystals of genistein under the crossed polarizers. It should be emphasized that there was no discernible liquid–liquid phase separation in this ternary mixture.

Fig. 8 exhibits a comparison between the liquid–liquid immiscibility gaps obtained for the unmodified PA/DMSO/water and genistein modified (PA/G)/DMSO/water systems. The liquid–liquid immiscibility gap for the modified system corresponds to 70/30 PA/G ratio. As illustrated in Fig. 8, the addition of genistein slightly enlarged the area of immiscibility gap, implying the reduced miscibility. Cloud point experiments were also conducted for other PA/G ratios such as 90/10 and 80/20. The data are not shown because the change in immiscibility area compared to the unmodified PA/DMSO/water was very small.

In the preparation of genistein modified membranes, the feed composition of genistein was varied and a series of membranes were formed by immersing into coagulation bath, during which some amount of genistein was lost in the non-solvent bath. Membranes were cast from the feed solutions with varying PA/G ratios of 90/10, 80/20, 70/30, 65/35 and 50/50. Therefore, it is imperative to know the actual genistein amount that is truly incorporated in the final membrane. The feed solution contained 17.5 wt % total solids, i.e., the weight of PA plus genistein relative to the DMSO. In order to quantify the amount of genistein lost (or genistein that was retained in the membrane), the non-solvent bath containing water, genistein, and DMSO were chilled at 15 °C for 96 h. During the cooling process, the genistein crystallized and precipitated out from the solution mixture, which were filtered, dried, and weighed. From a simple mass balance calculation, i.e., wt % of genistein = (wt of genistein) × 100/(wt of PA + wt of genistein), the actual amount of genistein in the final modified membrane was determined. As illustrated in Fig. 9, the higher the genistein loading in the feed solution, the higher was the loss during membrane formation. However, the genistein loading in the final membranes saturated out approximately at 35 wt% of the solid content against the dashed line representing the hypothetical situation where all genistein in feed were retained in the membrane after coagulation in the non-solvent.

One of the frequently employed hydrophilic polymers for fabricating hemodialysis membranes is PVP, which is often considered to improve biocompatibility of the membranes [25,26]. Controlling the PVP loading can optimize the hydrophilic/hydrophobic balance of the hemodialysis membranes to alleviate some, if not all, unfavorable interactions between blood proteins and the synthetic membranes. In order to quantify the actual amount of genistein retained in PA:PVP/G membranes, the coagulation bath containing water, genistein, PVP, and DMSO were chilled at 15 °C for 96 h to allow genistein to be crystallized first. The remaining solution was subsequently evaporated at 150 °C which left a residue that was predominantly made up of PVP. In this case, mass balance calculations included PVP weight, i.e., the wt % of genistein = (wt of genistein) × 100/(wt of PA + wt of PVP + wt of genistein). As can be seen in Fig. 9, the incorporation of PVP makes the actual amount of genistein in the final membrane to be considerably less because of the profound solubility of PVP in water, in which genistein is dragged out by the PVP leaching into the non-solvent bath.

The surface and cross-sectional morphologies of unmodified and genistein membranes examined by SEM are displayed Fig. 10 (a–d). A dense skin layer can be seen on the surface of the 100/0 PA/G (pure PA) membrane, whereas the cascading finger-like channels developed along the cross-section (Fig. 10(a)). The size of the cascading fingers progressively increases along the thickness direction from the skin layer (i.e., the top layer) where the solvent escapes and the non-solvent enters. The solvent/non-solvent that occurs during the course of membrane formation reduces the solvent quality progressively. As a result the homogeneous polymer solution becomes thermodynamically unstable and starts to phase separate into polymer-rich and polymer-poor phases. Phase separation takes place in the skin layer, which is the first surface to contact non-

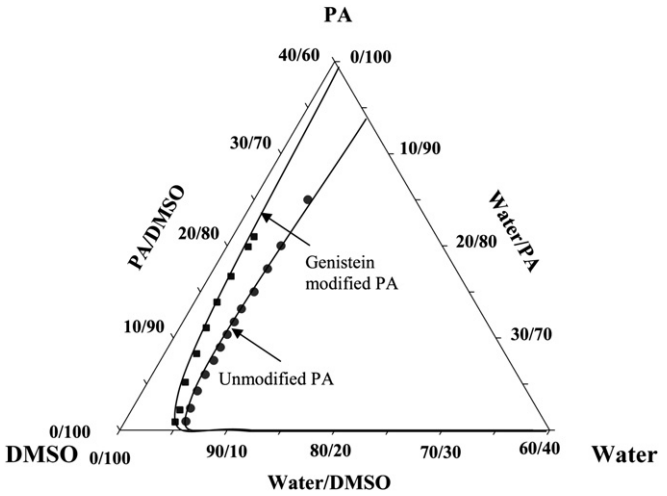

Fig. 8. Overlay of cloud point curves for unmodified PA (filled circles) and genistein modified PA (filled squares) in a mixture of DMSO and water, showing that the genistein addition resulted in enlargement of the liquid–liquid immiscibility gap. Each solution of modified system was prepared with PA/G ratio of 70/30.

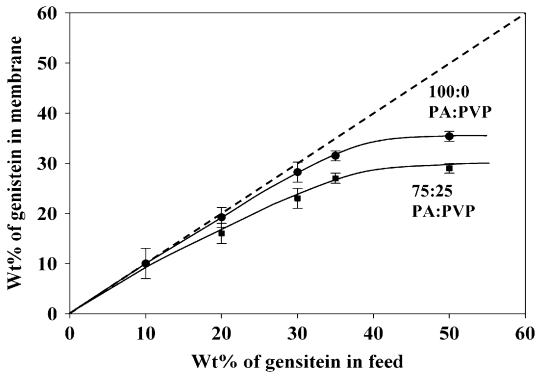

Fig. 9. Actual amounts of genistein retained in the final membrane in relation to amount of genistein in feed for various polymer blend ratios; 100:0 PA:PVP and 75:25 PA:PVP. Here the calculation was done using the following expression: wt % of genistein = wt of mangiferin × 100/(total wt of PA + PVP + genistein). Dashed line represents the ideal case in which all genistein in feed were retained in the final membrane.

solvent and the phase-separated domains serve as the point of entry for non-solvent into the film. As the non-solvent power is highest at the skin layer, it vitrifies quickly; therefore the size of the pores would be smaller at the film surface as seen in Fig. 10(a). As phase separation propagates inside the film, the non-solvent power becomes progressively poorer as the vitrified skin retards the influx of non-solvent. Consequently, more time is available for the phase separated porous structure to grow progressively at the late stages of coagulation driven phase separation, forming an asymmetric membrane with a cascading finger-like structure in the cross-sectional view of Fig. 10(a). It is reasonable to infer that the formation of cascading finger-like structures is governed by the changing solvent power at the coagulation front coupled with the hydrodynamic flow of solvent/non-solvent exchange that eventually creates the asymmetric membrane structure.

The effects of genistein modification on membrane morphology are illustrated in Fig. 10 (b–d). The striking effect of genistein modification is the formation of needle-like genistein crystals that are embedded on the membrane surface as well as in the cross-section even at very low feed composition of genistein (i.e., 90/10 PA/G). As the feed concentration of genistein was increased (for e.g., 80/20 and 70/30 PA/G), the resulting membranes contained larger dendritic crystals embedded on the membrane surface. The cross-sectional morphology of all the modified membranes revealed cascading finger-like channels except that the channels were loaded with genistein crystals (e.g., Fig. 10(c) and (d)). Increasing the genistein feed composition beyond 30 wt % resulted in the formation of larger spherulitic crystals on the membrane surface. However, it should be cautioned that higher genistein contents in the feed need not necessarily increase the actual

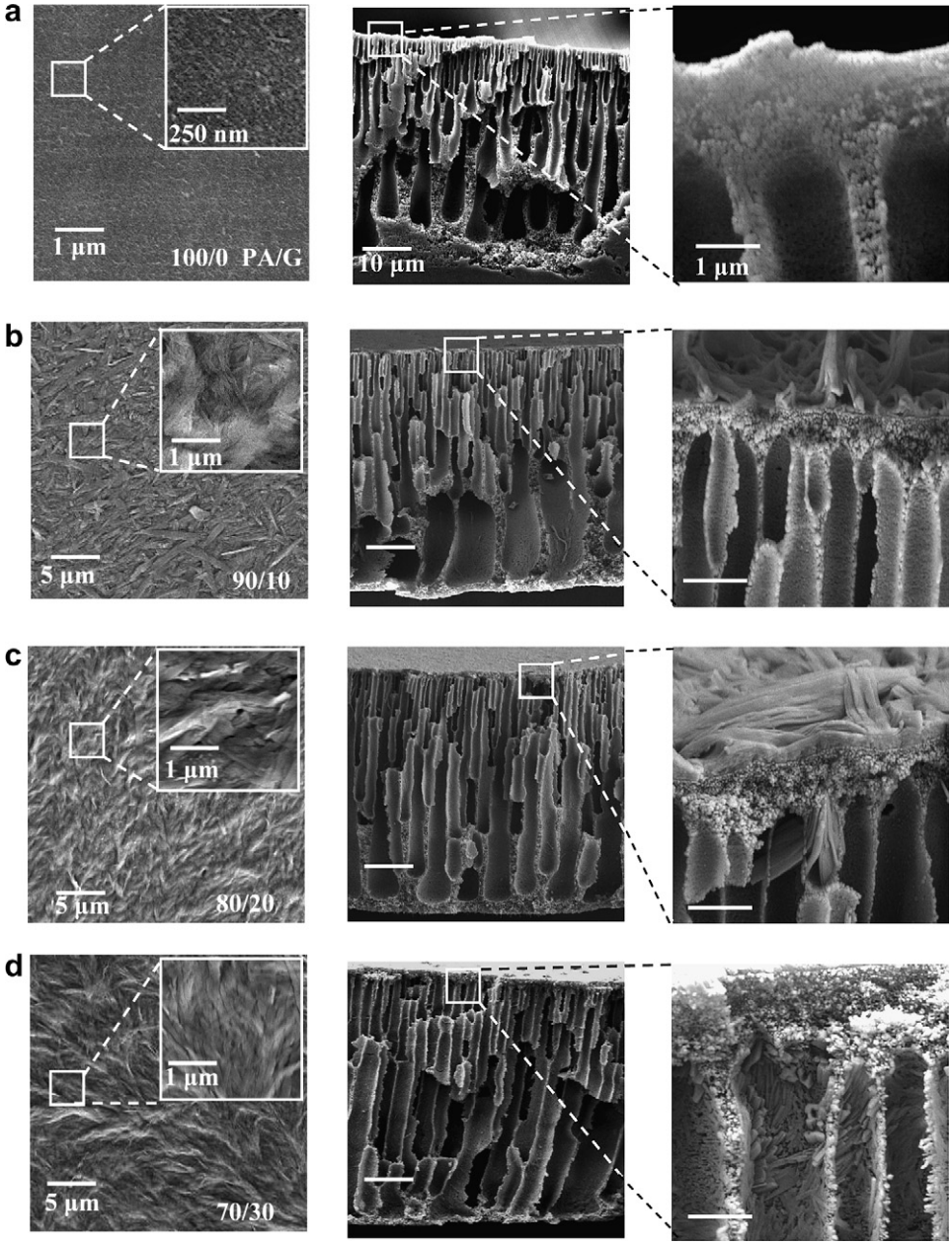

Fig. 10. SEM micrographs showing the surface (left column) and cross-sectional (right two columns) morphologies of the membranes with various PA/G ratios: (a) 100/0, (b) 90/10, (c) 80/20, and (d) 70/30. Micrographs in the insets of left column represent higher magnification image of the surface. The genistein-modified membranes clearly show embedded genistein crystals on the membrane surface as well as cross-section.

genistein content of the final membranes, as demonstrated in the actual uptake data of genistein in the membranes (Fig. 9).

In order to elucidate the effect of PVP addition, PA:PVP/G membranes were prepared from the PA:PVP/G/DMSO feed solutions in which the composition of genistein was fixed at 30 wt % while the ratio of PA:PVP was systematically changed. The effects of PVP addition on PA/G membrane morphology are illustrated in Fig. 11 (a–c). It can be immediately noticed that the addition of PVP tends to suppress the formation of genistein crystals even at very low PVP concentrations (Fig. 11(a)) in comparison to Fig. 10(d). As PVP content is increased, fewer genistein crystals are observable on the membrane surface. At a higher PVP concentration (52.5:27.5 PA:PVP) (Fig. 11(c)), a large fraction of PVP was lost into the water bath, which in turn reduces the actual amount of genistein in the final membranes. In view of the partial miscibility between PVP and genistein, some genistein may be leached out together with the PVP during coagulation, although genistein itself is not soluble in water.

In order to qualitatively describe the coagulation pathway traversed by the system, a prism phase diagram was constructed as depicted in Fig. 12. In this plot, the top most triangular plane (i.e., plane 'a') represents the homogeneous solution of PA:PVP/genistein in DMSO, whereas the bottom most plane (plane 'e') represents various coexistence phases of the dry ternary blend of PA:PVP/genistein, which is exactly the same as shown in Fig. 6. Planes 'b', 'c', and 'd' are hypothetical planes that have been constructed in order to illustrate a plausible coagulation pathway for the PA:PVP/genistein membranes with changing solvent power. These hypothetical planes are represented by the dashed lines. Here plane 'd' represents the vitrification plane (i.e., the plane at which the system solidifies due to crystallization or falls below the glass transition temperature). The areas of various coexistence regions diminish progressively with increasing solvent quality, and eventually becomes a homogeneous solution when the solvent power is the highest like pure solvent (i.e., as we move from plane 'd' to plane 'a'). It may further be assumed that the area of the coexistence regions will not change once the system is vitrified due to lack of molecular mobility (i.e., as we move from plane 'd' to 'e') and also the drying process has little or no effect on the final membrane composition from the plane 'd' to 'e'.

As the homogeneous solution (plane 'a') is immersed into a non-solvent bath, solvent/non-solvent exchange occurs and the coagulation pathway passes through planes 'b', 'c', and 'd', in which the solvent quality declines progressively (or non-solvent power increases). The direction of reduction in the solvent power is depicted by the double line arrow along the right hand side of the prism phase diagram. This reduction in solvent quality drives the formation of various coexistence regions since water is a non-solvent for both PA and genistein. From the morphology analysis it was realized that genistein crystals were found embedded on the membrane surface even at very low genistein feed composition (i.e., 90/10 PA/G). With this knowledge, the hypothetical coagulation pathway for PA/G membrane formation was shown by the dash-dotted arrow inside the prism. During the formation of PA/G membranes, the initial point lies in the plane 'a' where the system is

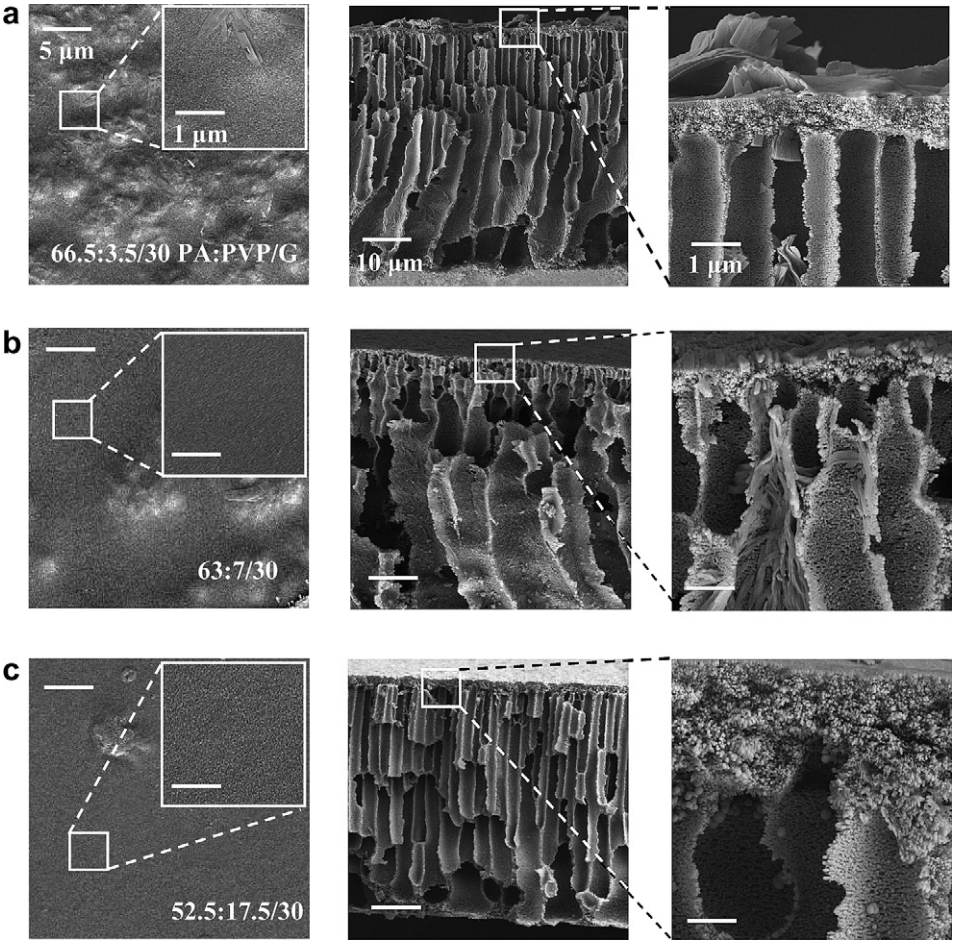

Fig. 11. SEM micrographs representing surface (left column) and cross-sectional (right two columns) morphologies of the membranes with the following PA:PVP/G ratios: (a) 66.5:3.5/30, (b) 63:7/30 and (c) 52.5:17.5/30. Micrographs in the insets of left column represent higher magnification image of the surface.

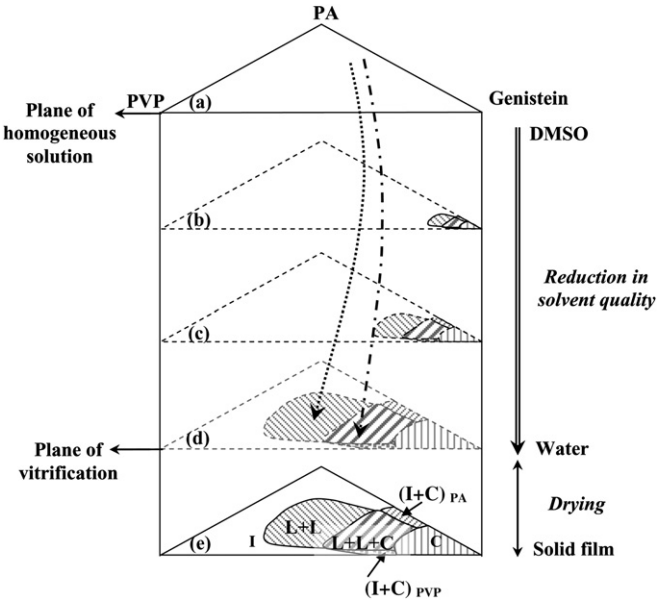

Fig. 12. A prism phase diagram illustrating the possible coagulation pathways represented by (—·▶) and (┈┈▶) traversed by the PA:PVP/genistein system during the course of membrane formation. The top most plane (plane 'a') represents homogeneous solution of PA:PVP/genistein with higher solvent concentration whereas plane 'd' represents the plane of vitrification. The intermediate planes 'b' and 'c' represent the hypothetical coexistence regions. The direction of reducing solvent power is indicated by a double line arrow. The phase boundary lines were drawn by hand to guide the eyes.

homogeneous. As the film is immersed into the non-solvent bath, the coagulation path drifts through the isotropic region within the plane 'b' and then enters the plane 'c' where the system begins to phase separate into polymer-rich (PA/G) and liquid-rich (DMSO/water) phases. As the coagulation pathway continues to move in the downward direction of the prism, the system reaches the plane 'd', which is the plane of vitrification, where the morphology of the system gets fixed since the long range motion of polymer chains is grossly restricted. Comparing the morphologies of the membranes in Fig. 10 with the prism phase diagram of Fig. 12, it can be inferred that the morphology of the membranes is fixed while crossing the liquid + liquid + crystal (L + L + C) coexistence gap; the genistein crystals thus formed are seemingly distributed in a phase separated matrix as manifested in Fig. 10(b–d). After vitrification and/or crystal solidification, the constituent molecules are no longer mobile and thus it is fair to hypothesized that the drying process at ambient temperature will not alter the coexistence regions of the phase diagram (i.e., from plane 'd' to 'e'). On the other hand, as PVP concentration is gradually increased in the feed solution, the coagulation pathway might enter the liquid–liquid coexistence region during the time of vitrification, thereby arresting the growth of genistein crystals. This alternate scenario is represented with a dotted line inside the prism phase diagram.

4. Conclusions

In summary, we have demonstrated, on the basis of FTIR, the occurrence of cross-hydrogen bonding between PA/G and PVP/G blends. The ternary phase diagram of PA:PVP/G was subsequently established that consisted of isotropic, liquid + liquid, isotropic + crystals, liquid + liquid + crystal and pure crystals of genistein. During coagulation, some genistein leach out into the non-solvent bath and the actual amounts of genistein retained in the final membranes were found to level off at 35 wt% genistein in feed in the PA/G membrane. This amount was reduced further to 30 wt% in the PA:PVP/G case because a larger amount of genistein was dragged out by PVP leaching into the non-solvent bath due to the profound solubility of PVP in water. Of particular interest was that the cascading finger-like channels were formed in the membrane cross-sections during coagulation driven by a competition between the liquid–liquid phase separation and the hydrodynamics of solvent/non-solvent exchange. This gradient cross-sectional porous channel with increasing diameters may be attributed to the changing solvent power of the solvent/non-solvent as the coagulation front propagates from the surface to the bottom substrate. Moreover, genistein crystals were found to be embedded on the surface as well as in the cross-section of the PA/G membranes even at a very low feed concentration of genistein. Potential implications of the embedded genistein crystals on the biomedical performance have yet to be explored. It may be conjectured that the genistein crystals can be retained in the membrane during hemodialysis, but only the surface of the crystals will be in contact with blood flow and thus its bioactivity and efficiency might have been compromised. In the PA:PVP/G membrane, the amount of genistein crystals was reduced with the addition of PVP, which may be attributed to greater miscibility between PVP and genistein. Finally, a possible coagulation pathway was drawn within a schematic prism phase diagram to qualitatively explain how the morphology of the final PA:PVP/genistein membranes might have emerged.

Acknowledgements

Partial support from University of Akron Research Foundation and Ohio Soybean Council is gratefully acknowledged.

References

[1] Mulder MHV. Basic principles of membrane technology. Dordrecht: Kluwer Academic Press; 1991.
[2] Hamilton RW. In: Henrich WL, Bennet WL, editors. Atlas of the diseases of the kidney, vol. 5. Massachusetts: Blackwell Publishing; 1999. p. 3.
[3] Daugridas JT, Blake PG, Ing TS. Handbook of dialysis. 4th ed. New York: Lippincott Williams and Wilkins; 2006.
[4] Galli F, Canestrari F, Bellomo G. In: Ronco C, La Greca G, editors. Vitamin E bonded membrane. A further step in dialysis optimization, vol. 127. Basle: Karger; 2003. p. 32.
[5] Nilsson B, Ekdalh KN, Mollnes TE, Lambris JD. Mol Immunol 2007;44:82–94.
[6] Bolch A. J Am Diet Assoc 1995;95:493–6.
[7] Meskin MS, Bidlack WR, Davies AJ, Omaye ST. Phytochemicals in nutrition and health. Boca Raton, FL: CRC Press; 2002.
[8] Bao Y, Fenwick R. Phytochemicals in health and disease. Basel, NY: Marcel Dekker; 2004.
[9] Wei H, Wei LH, Frenkel K, Bowen R, Barnes S. Nutr Cancer 1993;20(1):1–12.
[10] Kapiotis S, Hermann M, Held I, Seelos C, Ehringer H, Gmeiner BM. Arterioscler Thromb Vasc Biol 1997;17(11):2868–74.
[11] Puente J, Salas MA, Canon C, Miranda D, Wolf ME, Mosnaim AD. Int J Clin Pharmacol Ther 1996;34(5):212–8.
[12] Fiedor P, Kozerski L, Dobrowolzki JC, Kawecki R, Beniecki K, Pachecka J, et al. Transplant Proc 1998;30(2):537.
[13] Gohl H., Buck R., Strathmann H.. Basic features of the polyamide membranes. In Polyamide – the evolution of a synthetic membrane for renal therapy; Shaldon S., Koch K.M., Eds. Contrib Nephrol 1992, vol. 96, pp 1–25.
[14] Herold J, Meyerhoff G. Makromol Chem 1980;181:2625–36.
[15] Herold J, Meyerhoff G. Eur Polym J 1979;15:525–32.
[16] Neelakandan C, Kyu T. Polymer 2009;50:2885–92.
[17] Kuo SW, Chang FC. Macromolecules 2001;34:5224–8.
[18] Hu Y, Motzer HR, Etxeberria AM, Fernandez-Berridi MJ, Iruin JJ, Painter PC, et al. Macromol Chem Phys 2000;201:705–14.
[19] Skrovanek DJ, Howe SE, Painter PC, Coleman MM. Macromolecules 1985;18:1676–83.
[20] Chen TI, Kyu T. Polym Commun 1990;21:111–4.
[21] Kyu T, Chen TI, Park H, White JL. J Appl Polym Sci 1989;37:201–13.
[22] Skrovanek DJ, Coleman MM. Polym Eng Sci 1987;27(11):857–60.
[23] Vinogradov SN, Linnell RH. Hydrogen bonding. New York: Von Nostrand Reinhold; 1971.
[24] Ellis TS. J Appl Polym Sci 1988;36:451–66.
[25] Torres MR, Soriano E, Abajo J, de la Campa JG. J Membr Sci 1993;81:31–42.
[26] Kang JS, Lee YS. J Appl Polym Sci 2002;85:57–68.